1162 *Biochemistry* **2011,** *50,* 1162–1173
DOI: 10.1021/bi101435c

BIOCHEMISTRY
including biophysical chemistry & molecular biology
Article

Detailed Biophysical Characterization of the Acid-Induced PrP^c to PrP^β Conversion Process[†]

Trent C. Bjorndahl,[‡,§] Guo-Ping Zhou,[‡,§] Xuehui Liu,[‡] Rolando Perez-Pineiro,[‡] Valentyna Semenchenko,[∥] Fozia Saleem,[‡] Sandipta Acharya,[‡] Adina Bujold,[‡] Constance A. Sobsey,[‡] and David S. Wishart*[,‡,∥,⊥]

[‡]*Departments of Biological Sciences, and* [∥]*Computing Science, University of Alberta, Edmonton, Alberta, Canada T6G 2E8, and* [⊥]*National Institute for Nanotechnology, 11421 Saskatchewan Drive, Edmonton, Alberta, Canada T6G 2M9.*
[§]*These authors contributed equally to this work*

Received October 25, 2010; Revised Manuscript Received December 28, 2010

ABSTRACT: Prions are believed to spontaneously convert from a native, monomeric highly helical form (called PrP^c) to a largely β-sheet-rich, multimeric and insoluble aggregate (called PrP^{sc}). Because of its large size and insolubility, biophysical characterization of PrP^{sc} has been difficult, and there are several contradictory or incomplete models of the PrP^{sc} structure. A β-sheet-rich, soluble intermediate, called PrP^β, exhibits many of the same features as PrP^{sc} and can be generated using a combination of low pH and/or mild denaturing conditions. Studies of the PrP^c to PrP^β conversion process and of PrP^β folding intermediates may provide insights into the structure of PrP^{sc}. Using a truncated, recombinant version of Syrian hamster PrP^β (shPrP(90−232)), we used NMR spectroscopy, in combination with other biophysical techniques (circular dichroism, dynamic light scattering, electron microscopy, fluorescence spectroscopy, mass spectrometry, and proteinase K digestion), to characterize the pH-driven PrP^c to PrP^β conversion process in detail. Our results show that below pH 2.8 the protein oligomerizes and conversion to the β-rich structure is initiated. At pH 1.7 and above, the oligomeric protein can recover its native monomeric state through dialysis to pH 5.2. However, when conversion is completed at pH 1.0, the large oligomer "locks down" irreversibly into a stable, β-rich form. At pH values above 3.0, the protein is amenable to NMR investigation. Chemical shift perturbations, NOE, amide line width, and T_2 measurements implicate the putative "amylome motif" region, "NNQNNF" as the region most involved in the initial helix-to-β conversion phase. We also found that acid-induced PrP^β oligomers could be converted to fibrils without the use of chaotropic denaturants. The latter finding represents one of the first examples wherein physiologically accessible conditions (i.e., only low pH) were used to achieve PrP conversion and fibril formation.

Prions (PrP)[1] are endogenous, highly conserved membrane-bound proteins that are particularly abundant in the neuronal cells of vertebrates. Initially transcribed as an ~240-residue polypeptide with a 23-residue signal peptide, the mature form of PrP is an ~210-residue glycoprotein that is tethered to the cell surface via a glycosylphosphatidylinositol anchor at the C-terminus (*1*, *2*). While the physiological function of properly folded and processed PrP is not yet clear, it is now obvious that misfolded PrP can cause a variety of fatal neurodegenerative diseases in both animals and humans. These include scrapie in sheep, bovine spongiform encephalopathy (BSE) in cattle, and chronic wasting disease (CWD) in deer and elk, as well as Kuru, Creutzfeld-Jacob disease (CJD), and fatal familial insomnia (FFI) in humans (*3*, *4*). Collectively, these diseases are called transmissible spongiform encephalopathies or TSE's. Prions cause disease by converting from a soluble, helix-rich form (PrP^c) to an infectious β-rich form (PrP^{sc}) that is both insoluble and highly pathogenic (*5*). The process of conversion is still poorly understood, but several theories exist, including the "protein-only hypothesis", which is now widely supported by many lines of evidence (*5*, *6*). The underlying assumption of the protein-only hypothesis is that the presence of one or more PrP^{sc} molecules leads to the directed recruitment and one-way conversion of soluble PrP^c molecules into insoluble PrP^{sc}. An abundance of misfolded PrP^{sc} proteins within a neuronal cell or an organelle leads to the accumulation of amyloid protein deposits that eventually lead to cell death and the manifestation of neuronal disease (*6*, *7*).

PrP^c is soluble, monomeric mostly helical (43% α-helix, 5% β-sheet) protein that is easily susceptible to proteolytic cleavage from proteinase K. The three-dimensional structure of the native form of PrP^c was first solved in 1996 (*8*) and now more than 24 structures from many vertebrate species have been characterized by NMR and X-ray crystallography (*9*−*11*). The PrP^c fold appears to be highly conserved among all vertebrates and is characterized by three α-helices [helix H1, 143−156; helix H2, 173−195; helix H3, 200−226 (Syrian hamster numbering)] with

[†]This work was supported by grants from PrioNet and the Alberta Prion Research Institute (APRI).
*Corresponding author. E-mail: david.wishart@ualberta.ca. Phone: 780-492-0383. Fax: 780-492-1071.
[1]Abbreviations: ANS, 1-anilinonaphthalene-8-sulfonate; CD, circular dichroism; DLS, dynamic light scattering; DTT, dithiothreitol; MALDI, matrix-assisted laser desorption ionization; NMR, nuclear magnetic resonance; NOE, nuclear Overhauser effect; PrP, prion protein; PrP^c, native or cellular prion protein; PrP^{sc}, scrapie form of the prion protein; PrP^β, β-sheet-rich prion intermediate; shPrP, Syrian hamster prion protein; TCEP, tris(2-carboxyethyl)phosphine; TEM, transmission electron microscopy.

 Published on Web 12/28/2010

two small antiparallel β-strands (residues 127−130 and 162−165). The structure is stabilized by a disulfide bridge between Cys179 and Cys214, connecting helices H2 and H3. A large portion of the amino terminus (up to residue ~127) is disordered with no associated secondary structural elements (*12*, *13*).

While a great deal is known about the structure of the soluble or "native" form of PrP^c, somewhat less is known (or agreed upon) about the structure of PrP^{sc}. This is because the complex is large, insoluble, amorphous, and largely intractable to molecular characterization by conventional means such as X-ray crystallography and NMR spectroscopy. Nonetheless, several attempts using less conventional biophysical methods have been made to elucidate the structure of PrP^{sc}. These methods have increased our insight into possible structures but have also resulted in multiple, sometimes competing, models of the protein structure. Electron crystallographic studies of 2D crystals obtained from truncated PrP^{sc} fragments isolated from hamster brain tissue led to the development of an atomic resolution model characterized by a trimeric β-helix where the β-strand is largely localized to the N-terminus of the protein (*14*−*16*). Molecular dynamic studies by Daggett and colleagues, coupled with data from epitope mapping and other biophysical studies, produced a model of PrP^{sc} with similar N-terminal β-strand localization and trimeric stoichiometry but with a substantially different topology (*17*). Furthermore, recent studies by Surewicz and colleagues using mass spectrometry-based hydrogen/deuterium exchange and electron paramagnetic resonance of site-directed spin-labeled human PrP^{sc} fragments have provided solid evidence for a solvent-inaccessible, β-strand-rich core that maps to the C-terminus (residues ~160−220) instead of the N-terminus (*18*−*20*). This β-rich core is hypothesized to form single-molecule layers that stack on top of one another with parallel, in-register β-strands.

At this point it is unclear whether the discrepancies between these three PrP^{sc} models might be due to differences in protein constructs, sample preparation, sample conditions, and the analytical methods used for characterization or whether they may represent distinct differences between *in vivo* and *in vitro* forms of PrP^{sc}. Additional support for one (or more) of these models along with additional insight into the reasons for these differences might be gained by exploring the process by which PrP^c to PrP^{sc} conversion actually takes place and any associated intermediates. One such intermediate is PrP^{β}. PrP^{β} is a soluble, β-rich, oligomeric intermediate that can be easily generated using acidic pH and denaturing agents such as urea or guanidine (*21*, *22*) or high pressure (> 1.5 kbar) in mildly acidic conditions (*23*). Further work has shown that high concentrations of NaCl with urea also induced the formation of PrP^{β} (*24*). Studies by Baskakov and others (*25*, *26*) have shown that PrP (with its disulfide bond intact) can fold into either high-molecular-weight, insoluble amyloid fibers (at neutral pH, moderate denaturing conditions and agitation, PrP^{sc}) or a soluble form that is rich in β-sheets (at low pH, high salt and moderately denaturing conditions, PrP^{β}). Studies by O'Sullivan et al. showed that the PrP^{β} form could be generated from full-length murine PrP(23−231) using a combination of low pH (4.0), high salt (150 mM NaCl), and 3.5 M urea or, alternately, using low pH (4.0) and moderately high temperatures (37 °C) (*27*). Using CD and NMR spectroscopy, these researchers showed that PrP^{β} could be readily converted back to PrP^c by simply raising the pH to 5.2. They also showed that the protein converted to an apparent dimeric form that retained a largely unstructured N-terminus (up to residue 127) with most of the C-terminus evidently forming some kind of β-strand aggregate. Nearly identical results were also obtained with a full-length human prion construct (*28*). More recently, Surewicz and co-workers demonstrated that both the native and the D178N mutant of the human prion protein could be converted to fibrils without denaturing agents under mild acidic conditions (*29*).

Here we describe a detailed biophysical characterization of PrP^{β} and of the PrP^c to PrP^{β} conversion process using a combination of NMR, circular dichroism (CD), proteinase K digestion, mass spectrometry, dynamic light scattering (DLS), electron microscopy, and ANS fluorescence. In particular, we have found that it is possible to convert a recombinant Syrian hamster prion fragment shPrP(90−232) from PrP^c to PrP^{β} using only a simple pH titration (from pH 7.0 to pH 1.0) at low salt (20 mM) concentrations. This allowed us to obtain comprehensive $^1H/^{15}N$ assignments as well as detailed NOE, T_2, CD, and DLS data at multiple points throughout the conversion process. Our results implicate the flanking residues of the β-strand (B2) and the N-terminal residues of B1, H1, and H3 in the early stages of pH-induced conversion (as the pH drops from 5.2 to 2.8). These initial perturbations are followed by the aggregation of the protein below pH 2.8. The final and irreversible conversion occurs with the "locking down" of PrP^c to PrP^{β} at pH 1.0. Additional studies have shown that this acid-converted form of PrP^{β} is capable of forming PrP^{sc}-like fibrils through either the addition of salts or the reduction of the disulfide bond. This latter observation marks one of the first instances of using physiologically accessible conditions (i.e., only low pH or disulfide reduction) to achieve PrP conversion and fibril formation.

MATERIALS AND METHODS

Expression and Purification of Recombinant shPrP(90−232). A synthetic gene corresponding to residues 90−232 of the Syrian hamster prion including a 22-residue N-terminal fusion tag containing 6×-His and a thrombin cleavage site (MGSSHHHHHHSSGLVPRGSHML) was designed using codons optimized for *Escherichia coli* expression and synthesized by DNA 2.0 (Menlo Park, CA). The gene was cloned into a pET15b expression vector between *Xho*I and *Eco*RI restriction sites and heat shock transformed into the *E. coli* strain BL21 (DE3). The transformed cells were grown in 100 mL of LB plus 100 μg/mL ampicillin overnight to generate a starter culture. This starter culture was then used to inoculate 500 mL of M9 (^{15}N-labeled medium containing 1.0 g/L $^{15}NH_4Cl$) to an OD_{600} between 0.6 and 1.0 and set to shake at 225 rpm at room temperature for 1.5 h before induction with 1 mM IPTG. Twelve to eighteen hours later, cells were harvested by centrifugation at 3000 rpm for 25 min at 4 °C, resuspended in 6 M guanidine hydrochloride (100 mM K_2HPO_4, 10 mM reduced glutathione, pH 8.0), and subjected to five rounds of freeze/thawing. The lysate was cleared by centrifugation at 12000 rpm for 1 h and 45 min and then applied to 35 mL of nickel-NTA resin in a 3 × 15 cm column and allowed to bind to the resin at room temperature for 15 min. Subsequent removal of contaminants and on-column refolding (*30*) of the prion protein were achieved with 200 mL of wash buffer (8 M urea, 100 mM K_2HPO_4, pH 8.0) followed with a 200 mL gradient of 8−0 M urea (100 mM K_2HPO_4, pH 8.0). Residual contaminants were removed by washing the resin with 100 mL of 50 mM imidazole buffer (100 mM K_2HPO_4, pH 8.0), and the His-tagged prion protein was eluted with 500 mM

imidazole buffer (100 mM KH_2PO_4, pH 5.6). Fractions of 5 mL each were collected and screened with SDS−PAGE gels to determine purity. Because of the improved solubility characteristics, the lack of visible structure (by NMR), and the functional/structural similarity of the His tag to the N-terminus of native PrP, the N-terminal fusion tag was retained in all protein constructs described in this paper.

Preparation of NMR Samples. NMR samples were prepared at eight different pH values ranging from pH 1 to pH 5.2. Protein concentrations were calculated using a molar extinction coefficient of 25975 M^{-1} cm^{-1} at 280 nm. The purified prion proteins (~0.5 mM) at pH 5.2, 4.4, 3.5, and 3.2 were exchanged into 20 mM sodium acetate buffer. For pH values of 3.0 and 2.5, the protein was exchanged into 20 mM formic acetate. Buffer exchange was accomplished with successive rounds of volumetric dilution and concentrations in Ultrafree-15 centrifugal filter (Millipore) with a 3000 Da cutoff pour size. Ten percent (v/v) D_2O was added to each sample to maintain a spectral lock, 1 mM DSS (2,2-dimethyl-2-silapentane-5-sulfonate) was added for chemical shift referencing (*31*), and protein samples were transferred to Shigemi microcell NMR tubes (350 μL).

NMR Spectroscopy. NMR spectra were acquired at 30 °C on either a 500 or 800 MHz Varian Unity INOVA spectrometer fitted with either a 5 mm HCN *z*-gradient pulsed-field gradient (PFG) room temperature probe or an *xyz*-gradient PFG Varian cold probe, respectively. All experiments were conducted using Varian BioPack pulse sequences (VNMRJ v2.1B). 2D ^{15}N-HSQC spectra were acquired with 2048 complex points in the ^{1}H dimension and 256 complex points in the ^{15}N dimension with a recycle delay of 1.5 s. A total of 160 transients were collected for each experiment. 3D ^{15}N-edited NOESY-HSQC spectra (*32*) were collected at 800 MHz for the pH 5.2 sample. The spectral width was set to 8000 Hz for the directly and indirectly detected ^{1}H dimensions. A total of 2048, 224, and 72 complex points were collected in the t_2, t_1, and t_3 dimensions, respectively. For pH values of 4.4, 3.5, 3.2, and 3.0, 3D ^{15}N-edited NOESY-HSQC data were obtained with spectral widths of 6000, 6000, and 1800 Hz for the direct and indirect proton dimensions and the indirectly detected ^{15}N dimension, respectively. A total of 1024, 96, and 64 complex points were obtained in the t_2, t_1 and t_3 dimensions. Sixteen transients were collected using a mixing time of 150 ms for all NOESY experiments. ^{1}H−^{15}N TOCSY-HSQC (*33*) spectra were also obtained for protein samples covering the same pH range (4.4, 3.5, 3.2 and 3.0) at 500 MHz. For these spectra 1024, 96, and 64 complex points were collected for sweep widths of 6000 Hz, 6000 and 1400 Hz in the t_3, t_1, and t_2 dimensions, respectively. A total of 32 transients were averaged using a mixing time of 50 ms.

To assist with the assignment of ^{1}Hα resonances, HNHA spectra (*34*) were collected at 500 MHz for the samples at pH values of 5.2, 4.4, 3.5, 3.2, and 3.0. The HNHA spectra were obtained by averaging 32 transients. Sweep widths were set to 6000 Hz for each proton dimension and 1800 Hz for the ^{15}N dimension. A total of 1024, 110, and 64 complex points were collected in the t_3, t_1, and t_2 dimensions. All spectra were processed with NMRPipe (*35*) and analyzed with NMRViewJ (*36*). Vicinal $^3J_{HNHA}$ coupling constants were calculated from the HNHA spectra using NMRViewJ v1.1 and used to determine backbone φ angles (*34*). Backbone NOEs were obtained from the 3D ^{15}N-edited NOESY spectrum. NOE intensities were calibrated using NMRViewJ v1.1 and binned into strong medium and weak categories with upper bounds of 3.5, 4.5, and 6 Å, respectively.

Backbone amide T_2 rates were calculated from a series of HSQC spectra collected using 32 transients with 2048 complex points in the t_2 dimension, spanning 6000 Hz, and 128 increments in the t_1 dimension covering 1800 Hz. The transverse relaxation times were calculated with NMRviewJ v1.1 by fitting peak intensities from the ^{15}N HSQC spectra to the first-order exponential decay curve defined by $I_t = I_0e^{-t/T_2}$ using eight T_2 delays between 10 and 150 ms (20 ms intervals). The recycle time was set to 2.5 s.

Circular Dichroism Spectroscopy. All circular dichroism (CD) spectra were recorded in the far-UV region (190−260 nm) at 25 °C in a 0.02 cm path-length quartz cell on an Olis DSM 17 spectropolarimeter. The protein samples were prepared by dialysis whereby 0.5 mg/mL protein (pH 5.2) was exchanged into the buffers previously described for the NMR sample preparations (pH values of 4.4, 3.6, 3.2, and 2.8). For pH values of 1.7 and 1.0, the buffer solution was prepared with the addition of concentrated HCl in ddH_2O. Protein concentrations were calculated prior to and after CD spectral collection. Spectra were averaged over 10 individual scans using a bandwidth 1 nm. All CD spectra were smoothed with a 3 nm window, and the secondary structure content of each sample was calculated using the program CDPro (*37*).

Proteinase K Resistance Assay. The method used to assess proteinase K (PK) resistance was adapted from Bessen and Marsh (*38*). Specifically, proteinase K (Sigma Aldrich, St. Louis, MO) was dissolved in 0.1 M Tris-HCl, pH 8.0, to a concentration of 2.5 mg/mL. Native PrP^c was kept in 20 mM sodium acetate buffer (pH 5.2) and PrP^β that was prepared by incubating native PrP^c at pH 1.0 overnight and then dialyzed back to pH 5.2 in 20 mM sodium acetate buffer prior to the reaction. To each of the PrP samples was added a sufficient amount of solid urea to give a final urea concentration of 3.0 M. Proteinase K was then added to the PrP^β and PrP^c samples (using PrP to PK ratios of 250:1 and 500:1), and the samples were incubated for 1 h at 37 °C. Protein digestion was stopped with the addition of 1 mM phenylmethanesulfonyl fluoride (PMSF).

Fluorescence Spectroscopy of ANS Binding. ANS (1-anilinonaphthalene-8-sulfonate) was purchased from Sigma Aldrich (St. Louis, MO). Fluorescence spectra were recorded in 1 cm path-length Eppendorf UVette plastic disposable cells (Eppendorf AG, Hamburg, Germany) on a PTI spectrofluorometer (Photo Technology International). ANS was added to the protein samples (100 μg/mL) in the buffer systems described above at pH values of 1.1, 1.7, 2.8, and 5.2 and allowed to react for 30 min at 30 °C. Subsequently, the fluorescence of ANS was monitored using an excitation wavelength of 385 nm and an emission wavelength of 475 nm. Both the excitation and emission slits were 4 nm. Following these measurements, all protein samples were dialyzed back to pH 5.2 (20 mM sodium acetate) in Pierce Slide-A-Lyzer dialysis cassettes (7000 MWCO), and the ANS binding experiments were repeated to check for β conversion reversibility.

Dynamic Light Scattering. Dynamic light scattering measurements were carried out using the Zetasizer-Nanoseries (Malvern Instruments) with a 4.0 mW He−Ne laser (633 nm). Protein samples (1.4 mg/mL, 20 mM sodium acetate at pH 5.2, 4.4, 3.6 3.2, 2.8, 1.7, and 1.0) were prepared by overnight dialysis and then filtered extensively through a 0.22 μM ultrafilm filter (Millipore) prior to data collection to remove particulate matter. Each filtered sample was placed in a 1 cm path glass cuvette and measured at a constant temperature of 25 °C using an autopilot

Table 1: Changes in DLS and CD with Decreasing pH[a]

	diameter by DLS (nm)		secondary structure (CDPro, initial)		secondary structure (CDPro, recovery)	
pH	initial	recovery	helix (%)	β (%)	helix (%)	β (%)
5.2	3.1 ± 0.6		43	5	43	5
4.4	3.1 ± 0.6	3.1 ± 0.6	39	15	43	5
3.6	3.1 ± 0.6	3.1 ± 0.6	37	17	42	5
3.2	3.2 ± 0.7	3.1 ± 0.6	35	18	42	5
2.8	5.5 ± 2.5	3.1 ± 0.6	32	20	42	5
1.7	7.0 ± 0.4	7.0 ± 2.4	17	30	38	18
1.0	18.7 ± 1.8	13.0 ± 3.0	12	46	12	46

[a]DLS and CDPro recovery data collected after the protein was dialyzed back to pH 5.2.

function, with 25 measurements per sample. The diameters of the monomeric (PrP^c) and aggregated prion proteins were calculated as described previously (*39*, *40*) from an average of the calculated volume distribution. The samples were then returned to pH 5.2 by overnight dialysis, and the experiments were repeated to check for reversibility of the oligomeric process.

PrP Fibril Formation. Following the collection of CD spectra, the protein samples (~0.5 mg/mL) at pH 1.0, 1.7, 4.1, and 7.0 (20 mM sodium acetate) were diluted to 1 μM (500 μL) in the same buffer containing either 150 or 250 mM NaCl and dispensed into 1.5 mL Eppendorf tubes. The samples were agitated at 500 rpm, 37 °C. The formation of fibrils was monitored by TEM (described below) for up to 1 month. Follow-up experiments to investigate the influence of disulfide reduction on fibril formation were conducted with the addition of 1, 2.5, and 5 mM TCEP to reaction mixtures at pH 4.1 and 7.0 (20 mM sodium acetate, 150 mM NaCl). These samples were further split into two batches, and the fibril formation protocol was repeated at both 25 and 37 °C with shaking at 500 rpm. The protein concentration remained at 1 μM for all follow-up experiments.

Electron Microscopy. Two microliters of each PrP fibril sample was spotted onto 300 mesh grids and allowed to dry. Samples were rinsed with 5 μL of milli-Q H_2O and then negatively stained for 1 min with 4 μL of 1% uranyl acetate after which the excess staining solution was wicked away and the samples were rerinsed with another 5 μL of ddH_2O. After drying for 5 min, the disks were imaged using a Philips/FEI (Morgagni) transmission electron microscope (TEM).

MALDI Mass Spectrometry. Following 12% SDS−polyacrylamide gel analysis of the proteinase K digested PrP^β oligomers, the bands were excised and transferred to 1.5 mL Eppendorf tubes. The gel was fragmented and washed with 200 μL of 50% acetonitrile (2×) and 50% acetonitrile with 50 mM ammonium bicarbonate (pH 8.0, 2×). The gel mixture was spun down in a microcentrifuge, and the wash solutions were removed by pipetting between washes. Finally, the gel fragments were dehydrated with 100% acetonitrile for 5 min and dried by rotary evaporation. Samples were resuspended in 50 μL of 25 mM ammonium bicarbonate and split into two portions. Half was left without further workup to obtain masses of the resulting proteinase K fragments and the other half subjected to tryptic digestion. To the latter samples was added 2.5 mM DTT, and the mixture was incubated at 37 °C for 1 h. Following the reduction reaction, trypsin gold (Promega) was added to a final concentration of 1 μg/mL, and the reaction was allowed to proceed at 37 °C for 1 h. The resulting solutions from each sample were pipetted, evaporated to dryness, and resuspended in 5 μL of 50% acetonitrile containing 0.1% trifluoroacetic acid and 5 mg/mL sinapinic acid. A 100-well stainless steel target was prespotted with 0.5 μL of 5 mg/mL sinapinic acid in acetone−methanol (3:2) onto which 0.5 μL of sample was added. The target plates were loaded into an ABI Voyager Elite MALDI mass spectrometer, and spectra were obtained by averaging 150 shots acquired with an acceleration voltage of 25000 V and a grid voltage of 93%.

RESULTS

Oligomerization Status by DLS. The dynamic light scattering (DLS) data measured at various pH values from 5.2 to 1.0 show an increase of molecular size of the PrP protein once the pH drops below 3 (Table 1). Based on PDB coordinate data from two recent structures for the 90−231 fragment of recombinant Syrian hamster prion protein (1B10.pdb and 2PRP.pdb), the average monomeric diameter of the protein at pH 5.2 was estimated at 3.78 ± 0.94 nm. Our DLS results confirm that the protein remains monomeric from pH 5.2 to pH 3.2, with an average diameter of 3.08 ± 0.55 nm. However, as the pH is decreased to 1.7, the diameter increases, indicating oligomerization of the protein. At pH 1.7, the average diameter is 6.97 ± 0.38 nm. Using the formula

$$\mathrm{MW\ (kDa)} = (1.68 d_H)^{2.3394} \quad (1)$$

where d_H is the protein diameter in nanometers, an average molecular mass of 62.4 ± 8.3 kDa is obtained (*40*−*42*). Given that our construct has a molecular mass of 18.6 kDa, these data indicate that the oligomer appears to consist of three protein monomers. When the pH is dropped to 1.0, a dramatic increase in molecular size is observed in which the diameter increases to 18.7 ± 1.8 nm. This value corresponds to an oligomer with molecular mass of 628 kDa (33-mer) with a standard deviation between 495 and 779 kDa (27-mer to 42-mer). Although these numbers are divisible by three (corresponding to 9, 11, and 14 trimers) the identification of a discrete multimer that might form the basic multimeric complex for fibril formation is difficult to ascertain from thesse data alone. Further studies conducted by TEM indicate that the oligomers formed at pH 1.0 (after 1 week of incubation) had diameters exceeding 200 nm (Figure 9C), while oligomers formed at pH 1.7 (after 1 week of incubation) had diameters approaching 50 nm (data not shown). Given that the DLS data were collected within 24 h of conversion initiation and the TEM data were collected 1 week after conversion initiation, these findings indicate that the size of the oligomers changes over time. DLS data were also acquired on the samples after returning the sample to pH 5.2 (Table 1). Full recovery to a monomeric state was seen for all samples down to pH 2.8. However, the sample exposed to pH 1.7 showed only partial

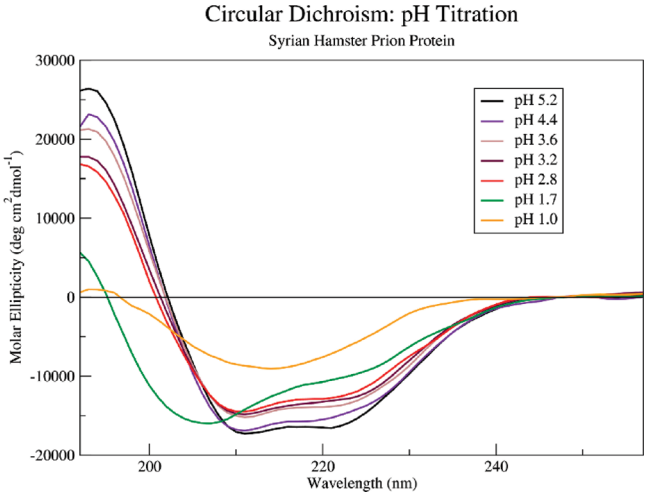

FIGURE 1: Circular dichroism spectra for the shPrP(90−232) construct at different pH values.

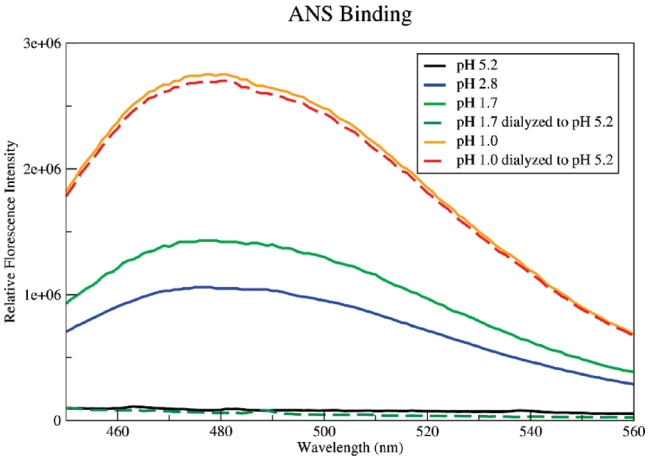

FIGURE 2: ANS fluorescence spectra upon binding to the shPrP-(90−232) construct at various pH values. Dotted lines represent the spectra collected following dialysis of the sample back to pH 5.2 in 20 mM sodium acetate buffer after overnight treatment at the various pH values.

recovery of a monomeric state while the sample exposed to pH 1.0 did not recover to a monomeric state.

CD Characterization of shPrP. CD spectra of the shPrP-(90−232) construct (Figure 1, Table 1) indicate a relationship between the protein's secondary structure content and the sample pH, so that as the pH decreases, the protein's α-helical content decreases and the β-strand content increases. This is consistent with previous pH-dependent CD studies (*43*). PrP^c samples exhibit a helical content of 43% at both pH 7.0 and pH 5.2, which is almost identical to the helical content calculated from the known 3D coordinates (44%; PDB 1B10). However, at pH 3.6, the α-helical content is reduced to 37% and the β-strand content increased to ∼17% (Table 1). This secondary structure content may reflect structural changes in the monomer alone, or (more likely) it represents a weighted contribution of a population of PrP monomers having native secondary structure and a small population of β-rich PrP^β oligomers. At pH 1.7, the helical content drops off dramatically to 17%, and the β-strand content increases to 30%. This likely reflects a dramatic increase in the proportion of small, β-rich PrP^β oligomers under these conditions. Despite the dramatic change in secondary structure content at this pH, the native structure can be recovered upon dialysis back to pH 5.2, where the CD curve returns to near its original shape so long as the larger oligomeric complex has not been allowed to form. These data suggest the β-oligomer (PrP^β) that is formed at pH 1.7 is quasi-stable or possibly a molten globule. However, with further reduction of the pH to 1.0, where only 12% of the helical structure remains and the β-strand content climbs to 46%, none of the original native structure is recoverable upon dialysis, even with short (less than 24 h) incubation times. At pH 1.0, the small portion of remaining helical content (as determined by CDPro calculations) can largely be attributed to β-turn structure, so the helix-to-β transformation of the protein is essentially complete at this pH. Evidently, pH 1.0 appears to be the "point of no return" in the conversion process where PrP^c has irreversibly converted to an oligomer comprised primarily of β-strand secondary structure.

ANS Fluorescence. ANS preferentially binds to the hydrophobic surfaces of proteins, leading to a substantial increase in fluorescence intensity (*44*). This feature has allowed a number of groups to characterize the unfolding process of PrP^c to PrP^β as buried hydrophobic side chains become solvent exposed during conversion (*25*, *45*). Our results (Figure 2) show that the affinity of ANS to the native, folded PrP^c protein at pH 5.2 is very low. However, as the protein is incubated in buffers with reduced pH values, a significant increase in ANS fluorescence intensity is observed. The moderate ANS binding to the PrP protein between pH 1.7 and pH 2.8 implies that there is some unfolding of the PrP^c protein or some dissociation of secondary structural elements of the protein such that the hydrophobic core is partially accessible (*46*). Despite the associated increase in fluorescence intensity with the drop in pH, all of the samples with pH values between 4.4 and 1.7 exhibit fluorescence spectra similar to the native PrP^c protein when dialyzed back to pH 5.2. However, the PrP^β protein treated at pH 1.0 shows the highest level of ANS fluorescence, which remains high even after dialysis back to pH 5.2. This indicates its native helical state could not be recovered. These data, along with our CD and DLS data, indicate that at pH 1.0 a significant portion of the protein's hydrophobic core is solvent exposed and the protein has been converted to an oligomer comprised mostly of β-strands.

Protease K Digestion Assay. Proteinase K (PK) has long been used to distinguish PrP^β (and PrP^{sc}) from PrP^c (*39*, *47*, *48*) as the hydrophobic residues generally recognized and cleaved in native PrP^c become occluded in the oligomeric form, making it more resistant to proteolytic digestion. Native gel analysis of the PrP^c protein in the absence of PK shows an expected band around 18 kDa, while the addition of PK results in complete digestion of the native PrP^c (Figure 3). However, when PK is incubated with PrP^β (1:500), additional bands are observed around 12 kDa, demonstrating that a fairly large segment of the PrP^β protein is at least partially resistant to proteolytic degradation with PK. Subsequent gel extraction and MALDI-MS and MS-MS analysis of these 12 kDa bands were performed to identify the PK-resistant fragment of the PrP^β protein. MALDI-MS analysis revealed fragment sizes of 12279 ± 332 and 11238 ± 161 Da for the upper and lower SDS gel bands, respectively. These masses correspond to a PrP fragment spanning from residue G131 to S232 (for the larger 12.3 kDa fragment) and a PrP fragment spanning from residue S132 to Y225 (for the smaller 11.2 kDa fragment). The smaller fragment was characterized by the loss of the C-terminal residues YDGRRSS and the loss of G131 on the N-terminus. Gel extraction, tryptic

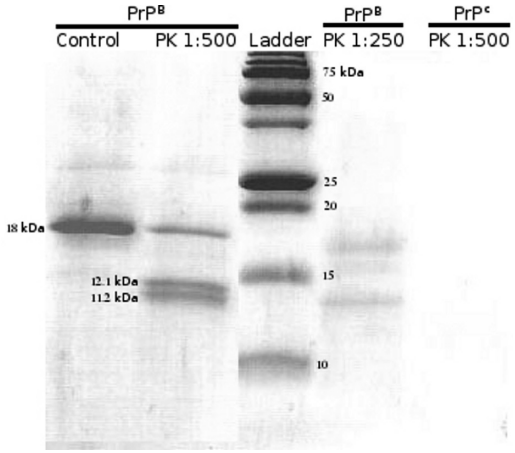

FIGURE 3: SDS−polyacrylamide gel (12%) for the native and acid-converted shPrP with proteinase K. Native shPrP^c is shown in lane 1 and after proteinase K digestion in lane 5. Proteinase K digestion of the acid-converted shPrP at two different concentrations is shown in lanes 2 and 4.

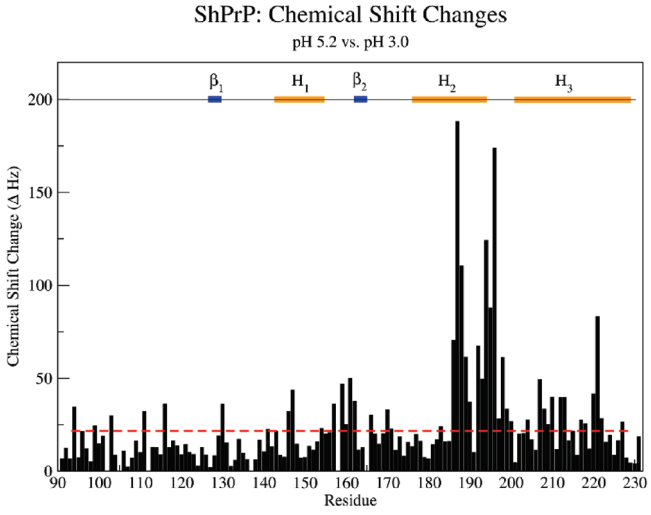

FIGURE 4: Chemical shift perturbations for the shPrP protein upon pH reduction from 5.2 to 3.0. Changes were calculated from the formula $\Delta Hz = |\nu HN_{pH5.2} - \nu HN_{pH3.0}| + |\nu N_{pH5.2} - \nu N_{pH3.0}| + |\nu H\alpha_{pH5.2} - \nu H\alpha_{pH3.0}|$/(no. of atoms used). The red line indicates the limit of digital resolution.

digestion of the two bands, and subsequent LC-MS analysis confirmed the disappearance of the tryptic C-terminal fragment "KESQAYYDGRRSS" for the 11.2 kDa band in the SDS gel, which agrees with the MALDI-MS findings. These results suggest all three of the helices and the β-strand B2 (spanning residues 132−225) are solvent-shielded after pH-induced oligomerization. Interestingly, these PK protection data for PrP$^\beta$ are also consistent with that reported for the PK-resistant core of PrP^{sc} (*49*−*52*).

NMR Characterization of PrP Conversion. Using the published ^{1}H−^{15}N-HSQC assignments of shPrP(90−231) in 20 mM sodium acetate (pH 5.2) at 25 °C (*13*), we assigned the ^{1}H−^{15}N-HSQC spectrum of our shPrP(90−232) construct at pH 5.2 (collected at 30 °C). From this spectrum, we were able to assign the remaining ^{1}H−^{15}N-HSQC spectra (collected at various pH values down to 3.0). Ambiguities, overlapped signals, and assignments for the 22-residue purification tag were resolved using 3D ^{15}N-TOCSY-HSQC, 3D ^{15}N-NOESY-HSQC, and 3D HNHA experiments. Complete ^{1}HN, ^{1}Hα, and ^{15}N resonance assignments were obtained for PrP samples at pH values down to 3.0. These assignments have been deposited into the BioMagResBank (BMRB accession no. 17034). Based on these assignments, ^{15}N-HSQC NMR spectroscopy was chosen to characterize the structure and dynamic behavior of shPrP(90−232). Since there was little chemical shift difference in the ^{15}N-HSQC spectra between pH 7.0 and pH 5.2 and because protein self-association and chemical exchange become particularly strong below pH 3.0 (as evident from DLS data, NMR signal loss, and line broadening for residues other than the unstructured N-terminal amino acids 90−120), we focused on comparing NMR data from pH values between 5.2 and 3.0. As the pH drops below 5.2, the regions encompassing residues Q186−T188 and K194−E196 exhibit large chemical shift changes (Figure 4). This finding mirrors previously reported results (*53*) that monitored changes of mouse prion (moPrP) down to pH 3.5. This mouse prion study indicated a drop in pH produces a tautomeric change in H186 that destabilizes the electrostatic network within this region of the protein. Recent work with various prion constructs containing disease-prone mutations in this region has further validated the significance of this destabilization (*54*). Interestingly, as the pH is dropped below 3.5, we began to observe additional chemical shift changes in other areas of the hamster protein. These have been mapped onto a ribbon diagram of the protein in Figure 5A. A number of additional amide perturbations were also observed for residues within the core of the protein between (around) helices H2, H3, and β-strand B2. As might be expected, when the protein begins to unfold, the core residues are the first to show signs of change. Apart from N143, additional residues show changes clustered in and around the putative steric zipper residues, including V166, N170, and E221 (*55*).

The molecular dynamics of PrP from pH 5.2 to pH 3.2 were characterized by measuring the ^{15}N T_2 values and corresponding $1/T_2$ (or R_2) relaxation rates (Figure 8A). A noticeable reduction in R_2 rates is observed for the unstructured N-terminal residues, for the residues in helix H2 (Q186 to N197), and for the residues in helix H3 (T215 to K220) (Figure 5). These changes indicate that these regions are experiencing faster motions as the solution becomes more acidic. The regions with the most significant increase in their R_2 rates also corresponded to those regions with the initial chemical shift perturbations highlighted in Figure 4. Interestingly, the other regions that showed chemical shift changes (N143, D144, N156 and additional residues within β-strand B2) exhibit changes in their R_2 rates. It has previously been shown that slow/intermediate chemical exchange exists within B2 for other prion constructs (*27*). Likewise, with our construct, comparison of 3D ^{15}N-NOESY-HSQC spectrum strip plots for residues in this region shows the same phenomenon in the same B2 region. An example for V161 at pH 5.2 and 3.2 is provided in the Supporting Information. Chemical shift analysis of these changes using the random coil index (RCI) (*56*, *57*), which is not sensitive to chemical exchange artifacts, indicates increased pico/nanosecond time scale fluctuations exist in the regions with the largest chemical shift perturbations only (Figure 8B). Those residues experiencing significant changes in their backbone amide dynamics are mapped onto the ribbon diagram presented in Figure 5B. Those residues exhibiting chemical shift changes upon continued reduction of pH correlate with those regions experiencing increased pico/nanosecond dynamic changes while other areas of the protein simultaneously present slower nano/microsecond dynamics or slower, intermediate chemical exchange (Figure 5A).

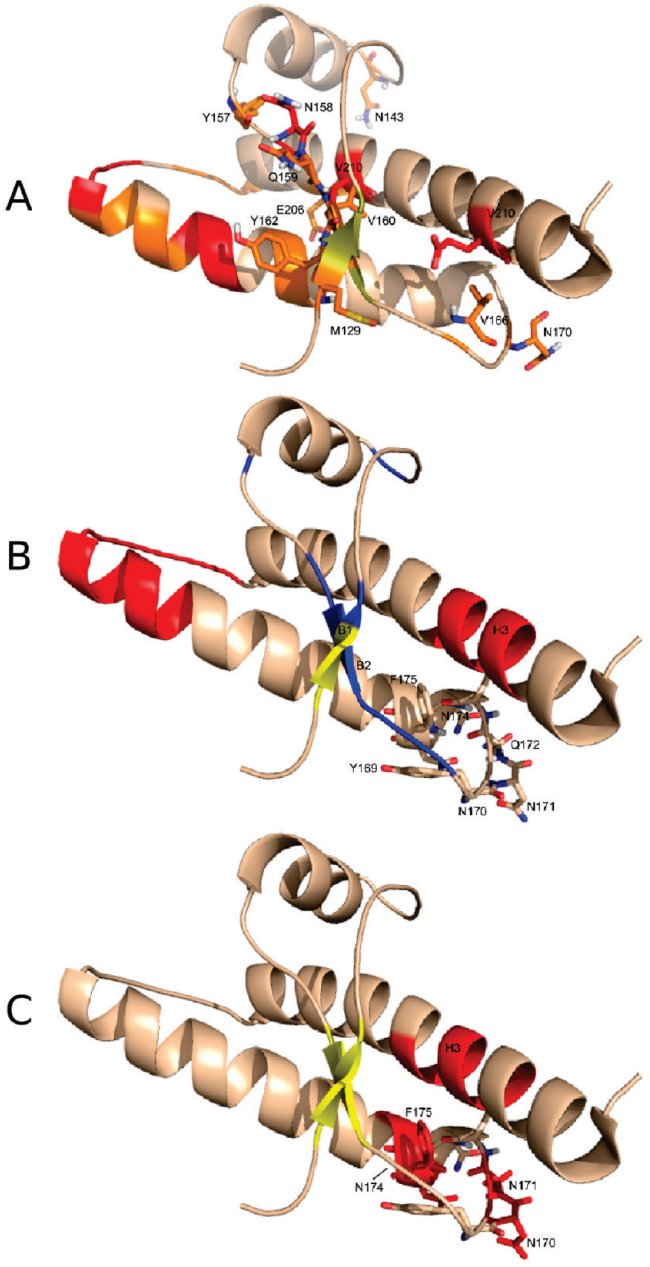

FIGURE 5: Ribbon representations of the shPrP (1B10.pdb). β-Strands are colored yellow. (A) Mapped onto the structure are the chemical shift changes plotted in Figure 4. Significant changes (> 50 Hz) are shown in orange, while those greater than 100 Hz are shown in red. Residue positions for new perturbations upon reduction of pH below 3.5 are annotated. (B) Changes in R_2 ($1/T_2$) rates are colored red (faster at pH 3.2) and blue (slower at pH 3.2). The putative steric zipper region ($Y^{169}NNQNNF^{175}$) is annotated. (C) NOE changes within the putative steric zipper and line width broadening observed for residues in helix H3 are colored red.

Dynamic data perturbations, amide chemical shift changes, and line width broadening are useful tools for identifying regions of change; however, they do not necessarily indicate what is occurring at a structural level. Therefore, the pH-induced structural changes in our PrP samples were evaluated by analyzing backbone NOE and coupling constant data. Structural changes as measured by the chemical shift index (CSI) (*58*) show a disruption in the C-terminus of helix H2 and a slight increase in the stability of helix H1 as the pH drops from 5.2 to 3.2 (Figure 6). Additionally, the NOE data indicate backbone structural changes also occur for residues within the prion protein's putative

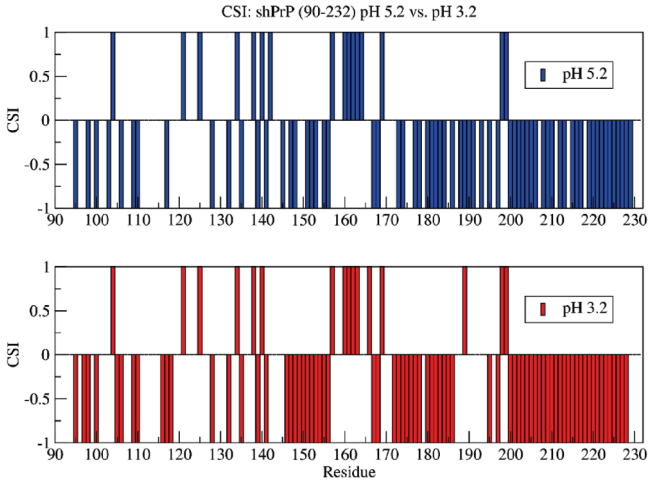

FIGURE 6: CSI plots for shPrP protein at pH 5.2 and 3.2.

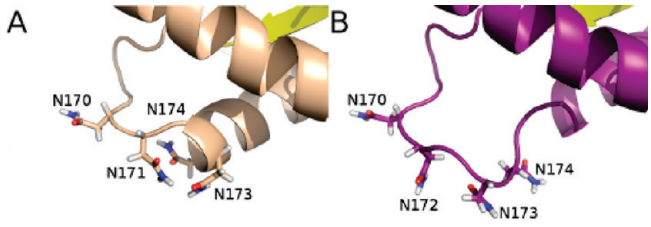

FIGURE 7: Structural model satisfying the backbone changes in the N-terminal cap of helix 2 upon decreasing the pH from 5.2 to 3.2.

"amylome motif" or amyloid-inducing motif (*59*). Specifically, residues N170, N171, Q172, N174, and F175 show altered NOE intensities (Figure 7). Based on these NOE intensity changes, there is a repositioning of the N171 backbone amide away from the backbone amide of Q172 and toward N170, while the amide from F175 moves closer to the amide of V176. Likewise, there is a loss of intramolecular NOEs from the backbone amide of N174 to its side-chain amide. These changes are shown in Figure S3, provided in the Supporting Information. While this loss of NOE intensity could result from a repositioning of the N174 side chain, it could also reflect dynamic changes (i.e., increased mobility of the N174 side chain). Evidence supporting these dynamic changes is provided by studying the adjacent residues in helix H3, many of which exhibit increased ^{15}N-HSQC line widths (Figure 8C). Helix H3 is positioned such that it has direct contact with those residues flanking the steric zipper motif. Additional evidence supporting these dynamic changes was observed from the signal loss in HNHA and ^{15}N-TOCSY-HSQC spectra for these same helix H3 residues when the pH was dropped to 3.0.

Fibril Formation. To examine whether fibrils (PrP^{sc}-like material) could be formed from our acid-induced PrP^{β} oligomers, we incubated the PrP^{β} samples at 37 °C, with shaking at 500 rpm. It has previously been argued that PrP^{β} oligomers are "dead-end" conformations and that fibrils could not be formed from PrP^{β} oligomers (*25*). Interestingly, with these pH-induced PrP^{β} oligomers, we found that fibrils could indeed be formed. While the presence of fibrils was noted after a few weeks of incubation at pH 1.0, the incubation time could be reduced by increasing by the concentration of NaCl to 250 mM (Figure 9D), leading to fibril formation within 1 week (~150 h). The initial fibrils or protofibrils could be described as small rod-like structures, 50−150 nm long and 10−20 nm wide. These protofibrils were generally observed in pairs and showed a right-handed twist every 40−60 nm.

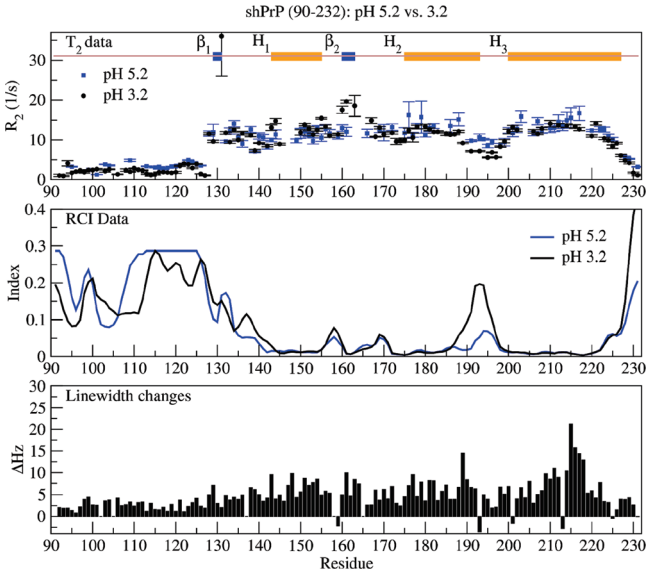

FIGURE 8: Graphs for R_2 ($1/T_2$), RCI, and line width changes upon reduction of pH from 5.2 to 3.2. (A) R_2 data for the shPrP at pH 5.2 (blue) and at pH 3.2 (black) recorded at 500 MHz. (B) RCI plots at pH 5.2 (blue) and pH 3.2 (black). (C) Changes in amide line widths upon reduction of the pH from 5.2 to 3.2.

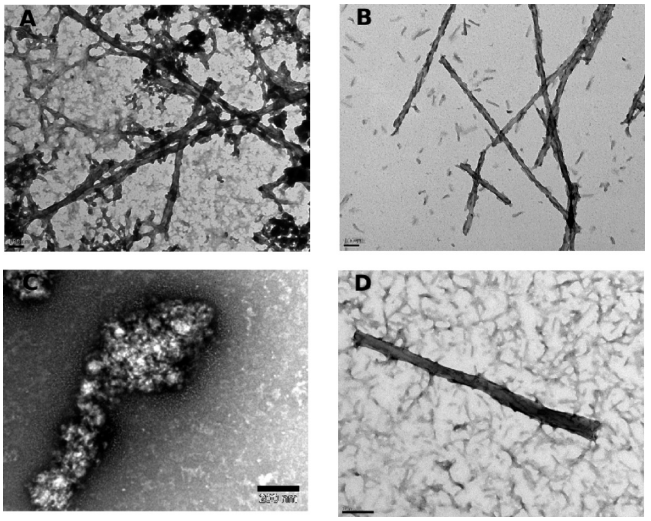

FIGURE 9: TEM pictures of shPrP fibrils formed under various conditions and times. Sixty-two hours (A) and 110 h (B) into fibril production in a reduced environment at pH 4.1 (20 mM sodium acetate, 125 mM NaCl, 1 mM TCEP). (C) β-Oligomers of the shPrP are shown after 1 week incubation. Oligomers were formed at pH 1.0. (D) Fibril formation after 1 week at pH 1.0 with 250 mM NaCl with 500 rpm agitation at 37 °C. The scale bars are 100 nm in panels A and B and 200 nm in panels C and D.

Over time, the fibrils further associated into much larger structures exceeding 1 μm in length and about 60 nm wide. The larger fibrils also exhibited a right-handed twist, and the short protofibrils were often seen to be associated with the longer fibrils in such a way so as to give a branched appearance to the assembly.

At pH 4.1 (37 °C, 500 rpm), our attempts to produce fibrils in a timely manner (< 1 week) were initially unsuccessful. However, upon reduction of the disulfide bond with TCEP, fibrils were readily attainable at this moderately low, but still physiologically attainable pH value. Initially, the oligomers grew to a diameter of about 200 mm. Self-association of these oligiomers ensued, and restructuring at the surface produced a tangled network of small protofibrils. The association of these protofibrils led to larger fibril-like structures that could be observed within 72 h (Figure 9A). Complete conversion into well-structured fibrils was evident after 110 h (Figure 9B). Extended incubation allowed the protofibrils to associate with the larger fibrils whose lengths could exceed 4 μm (data not shown).

DISCUSSION

The profound misfolding of the prion protein from a helix-rich form (PrP^c) to a β-sheet-rich form (PrP^{sc}) is the central event in the pathogenesis of spongiform encephalopathies (*5*, *6*, *48*, *60*−*62*). During this conversion, an intermediate form of the protein is believed to exist as a β-oligomer with molten globule-like properties (*63*, *64*). In this study, we have monitored and recorded the pH-driven conversion process of the native, α-helical rich PrP^c to the β-sheet-rich PrP^{β} form by collecting a series of ^{15}N-HSQC and CD spectra of the protein while dropping the pH from 5.2 to 1.0. Because no reducing agents, chaotropes (urea or guanidine), or high salt concentrations were used, as in previous studies (*65*−*68*), the conformational and dynamical changes of the protein depended solely on pH values. Although previous studies were able to obtain a β-sheet-rich structure under mildly acidic conditions (pH 3.9 to 3.6) in combination with high salt conditions or chaotropic agents, reversal of the conversion process was not evident upon subsequent dialysis against higher pH buffers. In this study, we were able to demonstrate reversibility, through dialysis, from pH values as low as 1.7. Furthermore, we were able to show that this conversion process continues to progress below pH 1.7, causing an irreversible "locking down" of the protein into a permanent β-oligomer at pH 1.0. The conditions necessary to generate this conversion indicate that the conformational transition from an α-helical protein to a β-sheet-rich isomer requires overcoming a large unfolding energy barrier.

Collectively, our CD and DLS data suggest that below pH 2.8 the protein begins to experience a helical unwinding or helix to β-sheet conversion. This secondary structure conversion coincides with an expansion of the protein's hydrodynamic diameter due to aggregation. At higher pH values (> 2.8), DLS data indicate that the protein remains monomeric, whereas T_2 data indicate that backbone fluctuations on multiple time scales are occurring for a number of residues within the protein core. Residues displaying significant chemical shift perturbations with increasing acidity experience faster motions, while the β-strands (B1 and B2) and the N- and C-terminal residues of helix H1 exhibit slower motions. These slower motions likely arise from intermediate conformational exchange processes (Figure 8A). A variety of conformational fluctuations have been noted for different regions of PrP protein constructs from other species (*27*), indicating these fluctuations are not exclusive to hamster PrP. Specifically, in a truncated form of mouse PrP, slow-to-intermediate exchange was noted for residues localized to the amylome motif loop region between B2 and H2. In our study, the most significant T_2 changes occurred within β-strand B2 and its flanking residues. This region is in direct contact with residues in helix H3, which also display significantly broadened amide signals. The mild discrepancies between mouse and hamster PrP might be due to small differences in construct design and/or experimental conditions. On a global scale, however, these fluctuations localize to a region of the protein that is adjacent to those residues displaying the most significant chemical shift perturbations.

Collective analysis of all of the NMR-derived data (chemical shift perturbations, line width changes, T_2 relaxation measurements, and NOEs) at pH 5.2 and 3.0 indicates that, with a drop in pH, changes are most evident in the region between β-strand B2 and helix H2 and adjacent residues in helix H3. This region runs through the core of the protein and includes the putative "amylome motif" region (NNQNNF), an area rich in hydrophilic residues, which is thought to be capable of forming a steric zipper (*53*, *58*). While changes in backbone chemical shifts and dynamics within the protein core are expected during protein unfolding, the changes near and within the putative amylome motif, prior to β-sheet conversion and oligomerization, are noteworthy. Consistent with the self-propagation theory, an exposed region or regions of the prion protein would have to exist in both the converted and unconverted prion proteins to facilitate self-association and structural conversion. Coincidently, the amylome motif lies within an exposed loop between H2 and H3 and is adjacent to H3, which contains a majority of the disease-associated mutations (*69*).

While coordinated changes in amide chemical shifts or backbone T_2 values can indicate regions of potential conformational change, they do not necessarily signal similar events. This is because amide proton shifts are sensitive to changes in hydrogen bond geometry or local electric fields while amide T_2 values are influenced by changes in backbone motion or flexibility. Each of these effects has been identified in this study, but neither effect can provide precise geometric information about the pH-induced structural changes. Therefore, direct observation of a structural change (via NOEs) provides a somewhat more meaningful interpretation of these changes. Here we provide such evidence. In particular, the unwinding of helix H2 is clearly suggested by backbone amide NOE changes that occurred going from pH 5.2 to pH 3.2. To further assess these changes, model 1 from PDB file 1B10.pdb (*13*) was refined using Xplor-NIH v2.25 (*70*, *71*) with the NOE data shown in the Supporting Information. A representative structure satisfying these NOE changes is presented in Figure 7. Specifically, the increased NOE intensity between $N170_{HN}$ and $N171_{HN}$, $N171_{HN}$ and $N170_{H\alpha}$, and $F175_{HN}$ and $V176_{HN}$ is accompanied by the loss of NOE intensity between the backbone amide of N174 and the α proton of N173 and the side-chain amide protons of N173 and N174. These changes are consistent with the unwinding of the N-terminal cap of helix 2. As seen in Figure 7, a number of stabilizing hydrogen bonds with the N-terminal cap are lost when the side chains of N173 (HD_{21}, 7.60 ppm) and N174 (HD_{11} and HD_{21}, 7.17 and 8.00 ppm) reposition themselves out into the solvent and the helix begins to unravel. These changes in backbone geometry were further confirmed by measuring changes in the $^3J_{HNH\alpha}$ coupling constants for residues Y169 (9.1−11 Hz), N173 (5.3−6.8 Hz), and N174 (6.1−8.1 Hz). While previous studies identified the region between helix 2 and helix 3 as the region undergoing initial pH-induced perturbations (*53*), these new data clearly identify this amylome region as the next region to undergo a change as the pH is further titrated below 3.5. It is noteworthy that instability in this region of the protein, specifically residues 173−179, was recently identified through high-pressure NMR studies (*72*).

Over the past decade there have been numerous accounts of perturbations and dynamic changes in various prion protein constructs; however, to our knowledge this is the first direct evidence of conformational change in an area of the prion protein proceeding to β-oligomerization. More significantly, our results were obtained under physiologically attainable conditions (pH 3) as opposed to physiologically unattainable conditions such as high pressure (>1.5 kbar), high temperature (>60 °C), or chemically denaturing conditions (3 M urea). It is also noteworthy that the repositioning of the side chains of N173 and N174 away from the N174 backbone amide appears to indicate that the formation of a steric zipper precedes dimerization of the protein. If this is indeed the case, one could hypothesize that ligands capable of stabilizing this region of the protein or interfering with the steric zipper formation could be highly effective at preventing oligomerization and/or subsequent fibriliziation.

While the NMR data allow us to identify which regions in the monomeric protein are experiencing conformational changes above pH 2.8, the CD data indicate that below pH 2.8 the protein begins to experience a clearly detectable helical unwinding or helix to β-sheet conversion. CD data collected at pH 2.8 reveal a modest (∼10%) conversion of secondary structure, while the DLS data indicate the protein is still largely monomeric. The extent of helical to β structure conversion was assessed in relation to the oligomerization process with the simultaneous analysis of CD and DLS data throughout the pH titration (Table 1). It is known that the unstructured N-terminal residues (90−120) are required for fibril formation, yet after fibril formation these residues are accessible to proteinase K digestion. This information suggests that these residues may play in important role only in the preliminary stages of self-recognition and aggregation. Although there are a sufficient number of residues in this flexible region that could account for the 25% shift in secondary structure content (if they were to associate in a β-strand conformation upon self-association), all of the evidence presented in this study suggests this does not happen. Rather, our NMR findings suggest that the structured helical core converts to a β-sheet upon self-association. This is also consistent with data collected by Surewicz and colleagues (*19*).

At pH 2.5, the C-terminal domain of the protein is likely experiencing slow or intermediate conformational exchange and is in equilibrium between a monomeric and oligomeric state (a "molten" oligomer). This is inferred by ^{15}N-HSQC spectra collected at pH 2.5, 1.7, and 1.0 that are largely devoid of any C-terminal domain signals (data not shown). Our DLS data indicate that the hydrodynamic radius of the protein at pH 1.7 corresponds to a trimer, and the only NMR-visible residues of the protein are found in the random coil N-terminus. This clearly indicates that the N-terminus is moving freely or independently of the larger oligomer. This quasi-oligomeric transitional complex at pH 1.7 exhibits an additional 15% increase in β-strand content over the β-strand content at pH 2.8. Reversible unfolding of this pH 1.7 complex is still possible so long as the protein solution remains dilute and it is not left in these low pH conditions for more than 24 h.

While pH 1.7 marks a point of significant structural rearrangement, it is at pH 1.0 that complete and final conversion is achieved. As measured by CD, the acid-induced PrP^{β} exhibits an almost exclusively β-strand conformation (>40% β-sheet) with only 12% of the protein consisting of a mix of helices or β-turns. At this point, none of the helical structure is recoverable following dialysis into buffer at pH 5.2. Other pH studies have reported irreversible conversion of the human prion protein at pH 4.1 (*28*). However, these studies used higher protein concentrations in chaotropic (i.e., 2 M urea) buffers with NaCl concentrations exceeding 150 mM. Our findings were recorded with lower protein concentrations (∼0.5 mg/mL) in "natural"

buffers devoid of urea. With our constructs any addition of salt at lower pH values, especially below pH 3.0, was found to induce protein aggregation that would prevent detailed NMR analysis. After overnight treatment at pH 1.0, the β-rich protein is proteinase K resistant and has a hydrodynamic diameter of 18.7 nm (corresponding to an estimated molecular mass of ~628 kDa or an aggregate of about 33 monomers).

Unlike the majority of previous protocols for fibril formation that require the use of nonphysiological denaturing/converting agents (SDS, urea, high salt, high temperatures), these findings suggest that fibrils could be induced to form in a low pH environment, like the stomach (pH 1.5−2) or the endosome/lysosome (pH 4), which was previously proposed as a site for conversion (*73*). Furthermore, the rate of this conversion was augmented with the addition of salt, possibly due to its ability to enhance the aggregation propensity of the prion protein at low pH values. Fibril formation with the human prion protein at moderate pH values (pH 4.1) without denaturing reagents has also been shown to be possible (*29*). While we were unable to form fibrils with our Syrian hamster construct at this pH, we were able to expedite fibril production after reducing the intramolecular disulfide bond with TCEP. In addition to construct differences, our conversion protocol was performed at 500 rpm, in keeping with previous reported protocols that utilized denaturants. Surewicz and co-workers made special note that the conversion was carried out at a very slow rotation rate (8 rpm), indicating that aggressive agitation may play a critical role in preventing the fibril formation under these mild, near-physiological conditions (*29*). In this study, we found that the fibrils formed under reduced conditions retained their structural integrity despite continued shaking at 500 rpm, whereas the fibrils produced under strongly acidic-only conditions (pH < 2.0) readily broke apart into their smaller protofibrilar structures. How and why reduction of the intramolecular disulfide bond might overcome these obstacles to facilitate fibril conversion with our construct and possibly affect fibril integrity are still undetermined. Another noteworthy finding is that the smaller protofibrils produced in a reduced environment appear to associate with the larger fibrils in a left-handed fashion (Figure 9B). This morphology varies from the acid-only generated fibrils reported here and other *in vitro* methods, which describe fibrils with a right-handed twist.

Despite the construct, procedural, and morphological differences in fibril formation, we have demonstrated that it is possible to overcome the energy barriers necessary for the conversion of the native protein to a β-oligomer and finally to fibrils under physiologic conditions like those found in the stomach or late endosome and that this possibility for conversion is not construct dependent.

CONCLUSION

In order to understand the process of structural rearrangement for the Syrian hamster prion protein, we developed a novel, pH-driven conversion process that converted the mostly helical protein (PrP^c) to a β-strand-rich form (both PrP^β oligomers and fibrils). This *in vitro* conversion process allowed us to perform a systematic, stepwise titration and to conveniently monitor these stepwise changes using a number of biophysical techniques. This study led to six major conclusions:

(1) CD, ANS fluorescence, and DLS showed that under low pH (< 3.0) and low salt (< 50 mM) conditions Syrian hamster PrP(90−232) can be converted to soluble, β-sheet-rich (> 40%) β-oligomers (PrP^β) that appear to consist of trimers (at pH 1.7) or multiples of trimers (pH < 1.7).

(2) CD and DLS showed that these pH-induced PrP^β oligomers can be reversibly refolded to native PrP^c if the pH remains above pH 1.0. If the pH drops below 1.0, the PrP^β oligomers become "locked", and PrP^c cannot be recovered.

(3) TEM studies showed that the PrP^β oligomers can be induced to form fibrils upon incubation with isotonic and supertonic buffers (150 and 250 mM NaCl, pH < 2.0) at physiologic temperature (37 °C) with agitation. These represent physiological conditions similar to what is found in the mammalian stomach (*74*).

(4) TEM showed that PrP^c could also be induced to form fibrils upon disulfide reduction with TCEP and incubation with isotonic and supertonic buffers (150 and 250 mM NaCl, pH 4.1) at physiologic temperature (37 °C) with agitation. These represent physiological conditions similar to what is found in the endosome.

(5) CD spectroscopy, NMR, protease K digestion, and MALDI-MS analysis indicate that the β-sheet structure and solvent-shielded components that appear upon pH-induced conversion of PrP^c to PrP^β are localized to the C-terminus (residues 131−225).

(6) NMR studies (chemical shift, NOE, T_2 relaxation, and line width analysis) of the early stages of pH-induced conversion revealed that the process begins with perturbations between helix H2 and helix H3 (pH 3.5) followed by changes to the protein core (helices H1 and H2, β-strand B2, and residues within H3) which flank the putative amylome motif region, $Y^{169}NNQNNF^{175}$, as the pH drops to 3.0. Furthermore, clear conformational changes are observed in the N-terminal cap of helix 2 that are consistent with helical unwinding and a loss of helical structure that was indicated from CD data. These findings indicate that the N- and C-termini of helix H2 are the first regions to experience conformational conversion and that these two areas could be of interest as possible therapeutic targets.

These six points essentially summarize the findings that differentiate this work from previously published studies. A few of our results also appear to reaffirm some previously disputed findings made with prions from different species. For instance, our β-sheet structure localization data (C-terminus as opposed to N-terminus) and fibril formation data are consistent with the results on human prions generated by the Surewicz group (*19*, *29*). It is also gratifying to see that the early events of the Syrian hamster prion pH conversion process (helix H2 and H3 destabilization followed by changes near the core of the protein) are similar to what was seen for the mouse prion (*53*). Overall, it must be emphasized that results from this study apply to a recombinant, truncated form of the Syrian hamster prion (no GPI anchor and no glycosylation) as studied *in vitro*. Whether these conclusions could apply to natural, full-length prions *in vivo* is unclear. Certainly, the biophysical features of our acid-converted PrP^β oligomers and fibrils (conversion of a helical protein to a β-sheet protein, protease K resistance, ANS binding, oligomeric structure, similar fibril dimensions and twist, etc.) resemble those seen in brain-derived PrP^{sc}. However, these pH-derived β-oligomers and amyloid fibrils (as with most *in vitro* converted PrP constructs) do not exhibit the catalytic self-propagation capabilities or the infectious properties of brain-derived PrP^{sc}. With the recent development of new sonication-based conversion methods to generate infectious PrP^{sc} from

truncated recombinant material (*75*), it would be interesting to see if these results translate to recombinant PrP^{sc}.

ACKNOWLEDGMENT

We thank the Canadian National High Field NMR Centre (NANUC) for assistance and use of the facilities. Operation of NANUC is funded by the Canadian Institutes of Health Research (CIHR), the Natural Science and Engineering Research Council of Canada (NSERC), and the University of Alberta. Additional thanks to Randy Mandryk for the collection of TEM data.

SUPPORTING INFORMATION AVAILABLE

Overlapped ^{15}N-HSQC spectra of the shPrP protein at pH 5.2 (black), pH 4.4 (blue), and pH 3.2 (red) (Figure S1); ^{15}N-HSQC-NOESY strip plots for V161 at pH 5.2 and pH 3.0 (Figure S2); strip plots for N170, N171, N174, and F175 at values of 5.2 and 3.2 (Figure S3). This material is available free of charge via the Internet at http://pubs.acs.org.

REFERENCES

1. Stahl, N., Borchelt, D. R., Hsiao, K., and Prusiner, S. B. (1987) Scrapie prion protein contains a phosphatidylinositol glycolipid. *Cell 51*, 229–240.
2. Stahl, N., Baldwin, M. A., Hecker, R., Pan, K. M., Burlingame, A. L., and Prusiner, S. B. (1992) Glycosylinositol phospholipid anchors of the scrapie and cellular prion proteins contain sialic acid. *Biochemistry 31*, 5043–5053.
3. DeArmond, S., and Prusiner, S. B. (2003) Perspectives on prion biology, prion disease pathogenesis, and pharmacologic approaches to treatment. *Clin. Lab. Med. 23*, 1–41.
4. Weissmann, C., and Aguzzi, A. (2005) Approaches to therapy of prion disease. *Annu. Rev. Med. 56*, 321–344.
5. Prusiner, S. B. (1996) Molecular biology and pathogenesis of prion diseases. *Trends Biochem. Sci. 21*, 482–487.
6. Prusiner, S. B. (1982) Novel proteinaceous infectious particles cause scrapie. *Science 216*, 136–144.
7. May, B. C., Govaerts, C., Prusiner, S. B., and Cohen, F. E. (2004) Prions: so many fibers, so little infectivity. *Trends Biochem. Sci. 29*, 162–165.
8. Riek, R., Hornemann, S., Wider, G., and Billeter, M. (1996) NMR structure of the mouse prion protein domain PrP (121−231). *Nature 382*, 180–182.
9. Lysek, D. A., Schorn, C., and Nivon, L. G. (2005) Prion protein NMR structures of cats, dogs, pigs, and sheep. *Proc. Natl. Acad. Sci. U.S.A. 102*, 640–645.
10. Calzolai, L., Lysek, D. A., and Pérez, D. R. (2005) Prion protein NMR structures of chickens, turtles, and frogs. *Proc. Natl. Acad. Sci. U.S.A. 102*, 651–655.
11. Pérez, D. R., Damberger, F. F., and Wüthrich, K. (2010) Horse prion protein NMR structure and comparisons with related variants of the mouse prion protein. *J. Mol. Biol. 400*, 121–128.
12. Riek, R., Hornemann, S., Wider, G., and Glockshuber, R. (1997) NMR characterization of the full-length recombinant murine prion protein, raPrP (23−231). *FEBS Lett. 413*, 282–288.
13. Liu, H., Farr-Jones, S., Ulyanov, N. B., Llinas, M., Marqusee, S., Groth, D., Cohen, F. E., Prusiner, S. B., and James, T. L. (1999) Solution structure of Syrian hamster prion protein rPrP(90−231). *Biochemistry 38*, 5362–5377.
14. Govaerts, C., Wille, H., and Prusiner, S. B. (2004) Evidence for assembly of prions with left-handed β-helices into trimers. *Proc. Natl. Acad. Sci. U.S.A. 101*, 8342–8347.
15. Boshuizen, R. S., Schulz, V., and Morbin, M. (2009) Heterologous stacking of prion protein peptides reveals structural details of fibrils and facilitates complete inhibition of fibril growth. *J. Biol. Chem. 284*, 12809–12821.
16. Walsh, P., Simonetti, K., and Sharpe, S. (2009) Core structure of amyloid fibrils formed by residues 106−126 of the human prion protein. *Structure 17*, 417–426.
17. DeMarco, M. L., Silveira, J., Caughey, B., and Daggett, V. (2006) Structural properties of prion protein protofibrils and fibrils: an experimental assessment of atomic models. *Biochemistry 45*, 15573–15582.
18. Lu, X., Wintrode, P. L., and Surewicz, W. K. (2007) β-Sheet core of human prion protein amyloid fibrils as determined by hydrogen/deuterium exchange. *Proc. Natl. Acad. Sci. U.S.A. 104*, 1510–1515.
19. Cobb, N. J., Sönnichsen, F. D., McHaourab, H., and Surewicz, W. K. (2007) Molecular architecture of human prion protein amyloid: a parallel, in-register β-structure. *Proc. Natl. Acad. Sci. U.S.A. 104*, 18946–18951.
20. Smirnovas, V., Kim, J. I., Lu, X., and Atarashi, R. (2009) Distinct structures of scrapie prion protein (PrPSc)-seeded versus spontaneous recombinant prion protein fibrils revealed by hydrogen/deuterium exchange. *J. Biol. Chem. 284*, 24233–24241.
21. Swietnicki, W., Petersen, R., Gambetti, P., and Surewicz, W. K. (1997) pH-dependent stability and conformation of the recombinant human prion protein PrP(90−231). *J. Biol. Chem. 272*, 27517–27520.
22. Hornemann, S., and Glockshuber, R. (1998) A scrapie-like unfolding intermediate of the prion protein domain PrP(121−231) induced by acidic pH. *Proc. Natl. Acad. Sci. U.S.A. 95*, 6010–6014.
23. Kuwata, K., Li, H., Yamada, H., and Legname, G. (2002) Locally disordered conformer of the hamster prion protein: a crucial intermediate to PrPSc? *Biochemistry 41*, 12277–12283.
24. Morillas, M., Vanik, D. L., and Surewicz, W. K. (2001) On the mechanism of alpha-helix to beta-sheet transition in the recombinant prion protein. *Biochemistry 40*, 6982–6987.
25. Baskakov, I., Legname, G., Baldwin, M. A., Prusiner, S. B., and Cohen, F. E. (2002) Pathway complexity of prion protein assembly into amyloid. *J. Biol. Chem. 277*, 21140–21148.
26. Bocharova, O. V., Breydo, L., and Salnikov, V. V. (2005) Synthetic prions generated in vitro are similar to a newly identified subpopulation of PrPSc from sporadic Creutzfeldt-Jakob disease. *Protein Sci. 14*, 1222–1232.
27. O'Sullivan, D. B., Jones, C. E., Abdelraheim, S. R., Thompsett, A. R., Brazier, M. W., Toms, H., Brown, D. R., and Viles, J. H. (2007) NMR characterization of the pH 4 beta-intermediate of the prion protein: the N-terminal half of the protein remains unstructured and retains a high degree of flexibility. *Biochem. J. 401*, 533–540.
28. Gerber, R., Tahiri-Alaoui, A., and Hore, P. J. (2008) Conformational pH dependence of intermediate states during oligomerization of the human prion protein. *Protein Sci. 17*, 537–544.
29. Cobb, N. J., Apetri, A. C., and Surewicz, W. K. (2008) Prion protein amyloid formation under native-like conditions involves refolding of the C-terminal α-helical domain. *J. Biol. Chem. 283*, 34704–34711.
30. Zahn, R., Liu, A., Lührs, T., Riek, R., Von Schroetter, C., López García, F., Billeter, M., Calzolai, L., Wider, G., and Wüthrich, K. (2000) NMR solution structure of the human prion protein. *Proc. Natl. Acad. Sci. U.S.A. 97*, 145.
31. Wishart, D. S., Bigam, C. G., Yao, J., Abildgaard, F., Dyson, H. J., Oldfield, E., Markley, J. L., and Sykes, B. D. (1995) ^{1}H, ^{13}C and ^{15}N chemical shift referencing in biomolecular NMR. *J. Biomol. NMR 6*, 135–140.
32. Kay, L., Keifer, P., and Saarinen, T. (1992) Pure absorption gradient enhanced heteronuclear single quantum correlation spectroscopy with improved sensitivity. *J. Am. Chem. Soc. 114*, 10663–10665.
33. Zhang, O., Kay, L. E., Olivier, J. P., and Forman-Kay, J. D. (1994) Backbone ^{1}H and ^{15}N resonance assignments of the N-terminal SH3 domain of drk in folded and unfolded states using enhanced-sensitivity pulsed field gradient NMR techniques. *J. Biomol. NMR 4*, 845–858.
34. Vuister, G. W., and Bax, A. (1993) Quantitative J correlation—A new approach for measuring homonuclear 3-bond J(H)(N)H(Alpha) coupling constants in N-15-enriched proteins. *J. Am. Chem. Soc. 115*, 7772–7777.
35. Delaglio, F., Grzesiek, S., Vuister, G. W., Zhu, G., Pfeifer, J., and Bax, A. (1995) NMRPipe: a multidimensional spectral processing system based on UNIX pipes. *J. Biomol. NMR 6*, 277–293.
36. Johnson, B. A. (2004) Using NMRView to visualize and analyze the NMR spectra of macromolecules. *Methods Mol. Biol.* (*New York*) *278*, 313–352.
37. Sreerama, N., and Woody, R. W. (2004) On the analysis of membrane protein circular dichroism spectra. *Protein Sci. 13*, 100–112.
38. Bessen, R. A., and Marsh, R. F. (1994) Distinct PrP properties suggest the molecular basis of strain variation in transmissible mink encephalopathy. *J. Virol. 68*, 7859–7868.
39. Georgieva, D., Koker, M., Redecke, L., Perbandt, M., Clos, J., Bredehorst, R., Genov, N., and Betzel, C. (2004) Oligomerization of the proteolytic products is an intrinsic property of prion proteins. *Biochem. Biophys. Res. Commun. 323*, 1278–1286.
40. Creighton, T. E. (1993) Proteins. Structures and Molecular Properties, W. H. Freeman, New York.

41. Janson, J. C., and Rydén, L. (1998) 3.3.1 estimation of molecular size by gel filtration, in Protein purification: Principles, high-resolution methods, and applications, pp 91−93, Wiley-VCH, New York.
42. Shaw, D., and Dubin, P. (2009) Aggregation of β-lactoglobulin, in Zetasizer nano application notes, pp MRK505-01, 1−3, Malvern Instruments, Worcestershire, U.K.
43. Matsunaga, Y., Peretz, D., Williamson, A., Burton, D., Mehlhorn, I., Groth, D., Cohen, F. E., Prusiner, S. B., and Baldwin, M. A. (2001) Cryptic epitopes in N-terminally truncated prion protein are exposed in the full-length molecule: dependence of conformation on pH. *Proteins 44*, 110–118.
44. Stryer, L. (1968) Fluorescence spectroscopy of proteins. *Science 162*, 526–533.
45. Safar, J., Roller, P. P., Gajdusek, D. C., and Gibbs, C. J. (1994) Scrapie amyloid (prion) protein has the conformational characteristics of an aggregated molten globule folding intermediate. *Biochemistry 33*, 8375–8383.
46. Semisotnov, G. V., Rodionova, N. A., Razgulyaev, O. I., Uversky, V. N., Gripas, A. F., and Gilmanshin, R. I. (1991) Study of the "molten globule" intermediate state in protein folding by a hydrophobic fluorescent probe. *Biopolymers 31*, 119–128.
47. Caughey, B., Raymond, G. J., and Bessen, R. A. (1998) Strain-dependent differences in beta-sheet conformations of abnormal prion protein. *J. Biol. Chem. 273*, 32230–32235.
48. Gerber, R., Tahiri-Alaoui, A., Hore, P. J., and James, W. (2007) Oligomerization of the human prion protein proceeds via a molten globule intermediate. *J. Biol. Chem. 282*, 6300–6307.
49. Prusiner, S. B. (1998) Prions. *Proc. Natl. Acad. Sci. U.S.A. 95*, 13363–13383.
50. Caughey, B., and Chesebro, B. (2001) Transmissible spongiform encephalopathies and prion protein interconversions. *Adv. Virus Res. 56*, 277–311.
51. Horiuchi, M., and Caughey, B. (1999) Specific binding of normal prion protein to the scrapie form via a localized domain initiates its conversion to the protease-resistant state. *EMBO J. 18*, 3193–3203.
52. Collinge, J. (2001) Prion diseases of humans and animals: their causes and molecular basis. *Annu. Rev. Neurosci. 24*, 519–550.
53. Bae, S. H., Legname, G., Serban, A., Prusiner, S. B., Dyson, H. J., and Wright, P. E. (2009) Prion proteins with pathogenic and protective mutations show similar structure and dynamics. *Biochemistry 48*, 8120–8128.
54. Gerum, C., Schlepckow, K., and Schwalbe, H. (2010) The unfolded state of the murine prion protein and properties of single-point mutants related to human prion diseases. *J. Mol. Biol. 401*, 7–12.
55. Sawaya, M. R., Sambashivan, S., Nelson, R., and Ivanova, M. I. (2007) Atomic structures of amyloid cross-beta; spines reveal varied steric zippers. *Nature 447*, 453–457.
56. Berjanskii, M., and Wishart, D. S. (2005) A simple method to predict protein flexibility using secondary chemical shifts. *J. Am. Chem. Soc. 127*, 14970–14971.
57. Berjanskii, M., and Wishart, D. S. (2008) Application of the random coil index to studying protein flexibility. *J. Biomol. NMR 40*, 31–48.
58. Wishart, D. S., Sykes, B. D., and Richards, F. M. (1992) The chemical shift index: a fast and simple method for the assignment of protein secondary structure through NMR spectroscopy. *Biochemistry 31*, 1647–1651.
59. Goldschmidt, L., Teng, P., Riek, R., and Eisenberg, D. (2010) Identifying the amylome, proteins capable of forming amyloid-like fibrils. *Proc. Natl. Acad. Sci. U.S.A. 107*, 3487–3492.
60. Pan, K. M., Baldwin, M., Nguyen, J., Gasset, M., Serban, A., Groth, D., Mehlhorn, I., Huang, Z., Fletterick, R. J., and Cohen, F. E. (1993) Conversion of alpha-helices into beta-sheets features in the formation of the scrapie prion proteins. *Proc. Natl. Acad. Sci. U.S.A. 90*, 10962–10966.
61. Safar, J., Roller, P. P., Gajdusek, D. C., and Gibbs, C. J. (1993) Thermal stability and conformational transitions of scrapie amyloid (prion) protein correlate with infectivity. *Protein Sci. 2*, 2206–2216.
62. Caughey, B., and Raymond, G. J. (1991) The scrapie-associated form of PrP is made from a cell surface precursor that is both protease- and phospholipase-sensitive. *J. Biol. Chem. 266*, 18217–18223.
63. Kelly, J. W. (1998) The alternative conformations of amyloidogenic proteins and their multi-step assembly pathways. *Curr. Opin. Struct. Biol. 8*, 101–106.
64. Surewicz, W. K., Jones, E. M., and Apetri, A. C. (2006) The emerging principles of mammalian prion propagation and transmissibility barriers: insight from studies in vitro. *Acc. Chem. Res. 39*, 654–662.
65. Weissmann, C. (1996) The Ninth Datta Lecture. Molecular biology of transmissible spongiform encephalopathies. *FEBS Lett. 389*, 3–11.
66. Lee, S., and Eisenberg, D. (2003) Seeded conversion of recombinant prion protein to a disulfide-bonded oligomer by a reduction-oxidation process. *Nat. Struct. Mol. Biol. 10*, 725–730.
67. Maiti, N. R., and Surewicz, W. K. (2001) The role of disulfide bridge in the folding and stability of the recombinant human prion protein. *J. Biol. Chem. 276*, 2427–2431.
68. Baskakov, I. V., Legname, G., Gryczynski, Z., and Prusiner, S. B. (2004) The peculiar nature of unfolding of the human prion protein. *Protein Sci. 13*, 586–595.
69. Prusiner, S. B. (1996) Transgenetics of prion diseases. *Curr. Top. Microbiol. Immunol. 206*, 275–304.
70. Schwieters, C. D., Kuszewski, J. J., Tjandra, N., and Clore, G. M. (2003) The Xplor-NIH NMR molecular structure determination package. *J. Magn. Reson. 160*, 66–74.
71. Brünger, A. T., Adams, P. D., Clore, G. M., DeLano, W. L., Gros, P., Grosse-Kunsteleve, R. W., Jiang, J. S., Kuszewski, J., Nilges, M., Pannu, N. S., Read, R. J., Rice, L. M., Simonson, T., and Warren, G. L. (1998) Crystallography and NMR system (CNS): a new software suite for macromolecular structure determination. *Acta Crystallogr., Sect. D 54*, 901–921.
72. Kremer, W., Kachel, N., Kuwata, K., Akasaka, K., and Kalbitzer, H. R. (2007) Species-specific differences in the intermediate states of human and Syrian hamster prion protein detected by high pressure NMR spectroscopy. *J. Biol. Chem. 282*, 22689–22698.
73. Mayer, R., Tipler, C., Laszlo, L., Arnold, J., Lowe, J., and Landon, M. (1994) Endosome-lysosomes and neurodegeneration. *Biomed. Pharmacother. 48*, 282–286.
74. Guyton, A. C., and Hall, J. E. (2006) Gastrointestinal physiology, in Textbook of Medical Physiology, 11th ed., p 797, Elsevier Saunders, Philadelphia, PA.
75. Wang, F., Wang, X., Yuan, C. G., and Ma, J. (2010) Generating a prion with bacterially expressed recombinant prion protein. *Science 327*, 1132–1135.